

## Peculiarities of anisotropy and polarization as an indicator of noises in the CMB maps

E. Kotok

*Theoretical Astrophysics Center, Juliane Maries Vej 30, 2100 Copenhagen, Ø Denmark  
August 2000*

P.Naselsky

*Theoretical Astrophysics Center, Juliane Maries Vej 30, 2100 Copenhagen, Ø Denmark;  
Rostov State University, Zorge 5, 344090 Rostov-Don, Russia*

D.Novikov

*Astronomy Department, University of Oxford, NAPL, Keble Road, Oxford OX1 3RH, UK;  
Astro-Space Center of P.N.Lebedev Physical Institute, Profsoyuznaya 84/32, Moscow, Russia*

I.Novikov

*Theoretical Astrophysics Center, Juliane Maries Vej 30, 2100 Copenhagen, Ø Denmark;  
Astronomical Observatory of the Copenhagen University, Juliane Maries Vej 30,  
2100 Copenhagen, Ø Denmark;  
Astro-Space Center of Lebedev Physical Institute, Profsoyuznaya 84/32, Moscow, Russia;  
NORDITA, Blegdamsvej 17, DK- 2100, Copenhagen, Denmark.*

We discuss some new problems of the modern cosmology which arose after the BOOMERANG and MAXIMA-1 successful missions. Statistics of high peaks of the CMB anisotropy is analyzed and we discuss possible inner structure of such peaks in the observational data of future MAP and PLANCK missions. We have investigated geometrical and statistical properties of the CMB polarization around such high isolated peaks of anisotropy in the presence of a polarized pixel noise and point sources. The structure of polarization fields in the vicinity of singular points with zero polarization is very sensitive to the level of pixel noises and point sources in the CMB maps.

PACS number(s): 98.80.Cq, 95.35.+d, 97.60.Lf, 98.70.Vc.

### I. INTRODUCTION

Observational data by BOOMERANG and MAXIMA-1 [1,2] open a new epoch in the investigation of the CMB power spectrum at the large multipole numbers  $l$ . The measured angular power spectrum shows a clear peak at angular scales corresponding to the spherical harmonic multipole number  $l \approx 200$ . This is the Sakharov's peak. However the structure of the CMB anisotropy power spectrum at  $l > 400$  is still unclear and next generation of satellite experiments (such as MAP and PLANCK) are needed.

There exist a few factors which play a leading role in the future experiments. Namely, both the MAP and PLANCK missions will provide significantly greater percentage of sky coverage than BOOMERANG and MAXIMA-1. In addition in the PLANCK mission there are two HFI channels  $\nu \simeq 545\text{GHz}$  and  $\nu \simeq 857\text{GHz}$  which provide  $FWHM = 5\text{arcmin}$  resolution. Future polarization measurements are also very important.

In contrast to BOOMERANG and MAXIMA-1 in both high frequency channels of PLANCK contamination foregrounds are of a prime consideration [3]. Of course, there is a wide variety of "technical" methods which could be applied to obtain a well-cleaned data over a wide range of angular scales. For example, one can use the frequency dependence of the various foregrounds (dust emission, synchrotron, thermal emission, point sources etc.) [3,4]. In practice this method meets serious difficulties because of the angular distribution on the sky and the frequency dependence of the foreground components are not well known.

That is why we would like to focus our attention on the investigation of local characteristics of the CMB anisotropy and polarization.

In this paper we analyze the statistics of the peaks (maxima and minima) in the CMB anisotropy maps. We compare this statistics for the BOOMERANG and MAXIMA-1 maps with the statistics for the future MAP and PLANCK observations and predict some properties of the peaks and their shapes in the future PLANCK observations. The main point of our attention is the analysis of the structure of the polarization field around singular points with zero polarization. We propose to use the results of the analysis for the estimation of the level of noise and foregrounds in the maps.

## II. STATISTICS OF PEAKS IN THE CMB ANISOTROPY MAPS

In this section we compare statistics of peaks (maxima and minima) for the BOOMERANG and MAXIMA-1 maps with the statistics for the future MAP and PLANCK observations.

Let us consider the model which is close to the real situation provided by the successful MAXIMA-1 balloon mission. According to [2] in the MAXIMA-1 pixelated map one can find a high amplitude peak in  $\Delta T/T$  distribution on the observed region of the sky with following coordinates: declination  $\simeq 58.6$  degrees; RA= 15.35 hours. In the Wiener-filtered map this peak has an amplitude  $\Delta T \sim 2.3 \div 2.5\sigma$  and it decreases monotonically down to  $1\sigma$  cross-level at  $15.2 < h \leq 15.4$  hours,  $58.5 < \delta < 60$  degree.

Below we predict some definite properties of the structure of such peaks in the future PLANCK CMB measurements performed with higher angular resolution than the current measurements. Analogous prediction has been done in [5] for the Tenerife Experiment using COBE DMR data although with the different technique. For example, we show that more accurate measurements will not reveal the inner structure of the peak in a form of new high ( $> 1.5\sigma$ ) peaks inside the area mentioned above. We assume that the fluctuations of the CMB anisotropy (or polarization) are realization of a random Gaussian process. It is well known that for such random processes all statistical properties of a signal are determined by the correlation function of the anisotropy

$$C_T(\theta) = \frac{1}{4\pi} \sum_l (2l+1) C_{l,T} W(l) P_l(\cos\theta), \quad (1)$$

where  $C_{l,T}$  is the power spectrum of fluctuations of anisotropy,  $W(l)$  is the window-function which depends on the strategy of the experiment,  $P_l(\cos\theta)$  are Legendre polynomials. Analogous expressions can be written for  $Q$  and  $U$  components of polarization:  $C_Q$  and  $C_U$ .

To investigate topology of the anisotropy and polarization maps we define the spectral parameters (as in [6,7])

$$\sigma_i^2 = (-1)^i i! 2^{2i} \frac{d^i C(0)}{d\omega^i}; \quad \omega = 2 \sin \frac{\theta}{2}; \quad (2)$$

$$\gamma(\theta_A) = \frac{[\sigma_1]^2}{\sigma_0 \sigma_2}; \quad \theta_* = \sqrt{2} \frac{\sigma_1}{\sigma_2}; \quad (\theta_C)^2 = -C(0) / \frac{d^2 C(0)}{d\theta^2},$$

where  $i = 0, 1, 2$ , and  $\theta_A$  is the antenna beam.

In the real experiments the antenna has a finite resolution and the spectral parameters depend on the antenna beam  $\theta_A$  and therefore on the number of Doppler peaks which could be resolved by the antenna. This means that in the future PLANCK maps the structure of the high  $\Delta T/T$  peaks can be different from the corresponding structure in the BOOMERANG and MAXIMA-1 maps.

For all cosmological models the power spectrum of the CMB anisotropy  $C_l$  can be described in terms of a sum of the Gaussian peaks centered at the points of the maxima  $l_n$ , ( $l \geq 30$ ) ([8])<sup>1</sup>

$$\frac{l(l+1)C_l}{2N\pi} = \left\{ \sum_n A_n \exp \left[ -\frac{(l-l_n)^2}{2d_n^2} \right] + 1 \right\} e^{-l^2 s^2}, \quad (3)$$

where  $n$  is the number of the peak,  $d_n$  is the width of the peak,  $l_n$  is its position,  $A_n$  is its amplitude and  $N$  is the normalization factor for low multipole range (for example, the COBE data normalization). The last term in Eq.(3)

---

<sup>1</sup>We will omit the index  $T$  in the subsequent discussions

accounts for the Silk-damping at the angular scale  $s$ . Note that we do not include in Eq.(3) any low and high multipole filters (the window function and beam). These means that Eq.(3) describes the initial power spectrum of fluctuations on the sky without any smoothing. In reality both last factors are extremely important and their influence on the  $\Delta T/T$  maps plays a crucial role. The power spectrum in the form of Eq.(3) after substitution into Eq.(2) gives information about the influence of each peak on the topology of  $\Delta T/T$  maps. Thus, using the approximate Eq.(3) we can investigate the influence of the first, second and subsequent Doppler peaks on the spectral parameters of the future maps of the MAP, PLANCK and other missions.

Next point is connected with the window function  $W(l)$  of the experiments. In a small angular approximation we will model general properties of  $W(l)$  as follows:

$$G(l) = \frac{W(l)}{l} = \exp[-l(l+1)\theta_A^2] \begin{cases} l^m & \text{if } l \ll 30 \\ l^{-1} & \text{if } l \gg 30, \end{cases} \quad (4)$$

where  $m = 2$  for the single difference and  $m = 3$  for the double difference scheme of the low multipole filtration. The exponent in Eq.(4) describes the antenna beam with  $\theta_A \simeq 7.45 \times 10^{-3}$  ( $\frac{\theta_{FWHM}}{1\sigma}$ ). For description of the asymptotes of the multiplier in Eq.(4) we can introduce a function which matches both limits

$$g(l) \simeq \frac{(lR)^{m+1}}{l[1 + (lR)^{m+1}]}, \quad (5)$$

where  $R \sim 0.03$  is the characteristic angular scale at the low multipole filtration [see Eq.(4)]. So, in such a model the spectral parameters in Eq.(2) are:

$$\sigma_i^2 = \int_0^\infty dl l^{2i} g(l) \left[ 1 + \sum_n A_n \exp\left(-\frac{(l-l_n)^2}{2d_n^2}\right) \right] e^{-l^2(s^2+\theta_A^2)}; \quad i = 0, 1, 2. \quad (6)$$

Note that for the second and higher Doppler peaks we have  $l_n^2/d_n^2 \gg 1$  and only for the first Doppler peak  $l_1^2/d_1^2 \simeq 5$ . For the analytical approximation of the integral in Eq.(6) we require the asymptotic  $l_n^2/d_n^2 \gg 1$  for all peaks in the power spectrum Eq.(3). Using this approximation we obtain the following result for the spectral parameters  $\sigma_i^2$ :

$$\sigma_0^2 = \frac{1}{2} \left\{ 2 \ln \frac{R}{\xi} - C + \sqrt{\frac{\pi}{2}} \sum_n A_n \frac{d_n}{l_n} \exp\left(\frac{-l_n^2 \xi^2}{1 + 2d_n^2 \xi^2}\right) \cdot (1 + 2d_n^2 \xi^2)^{1/2} \right\}, \quad (7)$$

$$\sigma_1^2 = \frac{1}{2\xi^2} + \sqrt{\frac{\pi}{2}} \sum_n \frac{A_n l_n d_n \exp\left(\frac{-l_n^2 \xi^2}{1 + 2d_n^2 \xi^2}\right)}{(1 + 2d_n^2 \xi^2)^{3/2}} \left[ 1 + \Phi\left(\frac{l_n}{d_n \sqrt{2(1 + 2d_n^2 \xi^2)}}\right) \right], \quad (8)$$

$$\sigma_2^2 = \frac{1}{2\xi^4} + \sqrt{\frac{\pi}{2}} \sum_n \frac{A_n l_n^3 d_n \exp\left(\frac{-l_n^2 \xi^2}{1 + 2d_n^2 \xi^2}\right)}{(1 + 2d_n^2 \xi^2)^{7/2}} \left[ 1 + \Phi\left(\frac{l_n}{d_n \sqrt{2(1 + 2d_n^2 \xi^2)}}\right) \right], \quad (9)$$

where  $C$  is the Euler constant,  $\xi^2 = \theta_A^2 + s^2$ ,  $\Phi(x) = 2/\sqrt{\pi} \int_0^x dx e^{-x^2}$  is the probability integral. As we can see from Eq.(7) only the first Doppler peak is important for calculation of the variance  $\sigma_0^2$ . The influence of the second and higher peaks is practically negligible due to the decrease of amplitudes  $A_n$  and  $d_n/l_n$ . However these peaks determine (see Eqs.(10)-(12)) the topological structure of  $\Delta T/T$  maps (for example, the number of maxima and minima at different thresholds  $\nu_n \sigma_0 = \Delta T/T$ ). Using Eqs.(8) and (9) we describe the realistic model at  $d_n^2 \xi^2 \ll 1$  and  $l_n^2 \xi^2 \leq 1$ . In such a model the density of all peaks at  $\nu \in (-\infty, \infty)$  has an especially simple form

$$N_{PK}^+ = N_{PK}^- = \frac{1}{8\pi\sqrt{3}} \frac{\sigma_2^2}{\sigma_1^2} (\text{ster})^{-1}, \quad (10)$$

where  $N_{PK}^+$  and  $N_{PK}^-$  are the densities of all maxima and minima correspondingly. The density of saddle points (of arbitrary high) is

$$N_{sad}(-\infty) = 2N_{PK}^+ (\text{ster})^{-1}. \quad (11)$$

Let us now discuss a model in which all Doppler peaks are smoothed ( $A_n = 0$ ). In such a model the spectral parameters  $\theta_*$  and  $\gamma$  are the following

$$\theta_*^2 = 2\xi^2; \quad \gamma = (2 \ln \frac{R}{\xi} - C)^{-1/2}, \quad (12)$$

and the densities of all maxima and minima (with arbitrary height) are  $N_{PK}^+ = N_{PK}^- = \frac{1}{8\pi\sqrt{3}}\xi^{-2}$ . If the sky coverage for some  $\Delta T/T$  - experiment is  $f_{sky}$  (for example,  $f_{sky} \simeq 0.3\%$  for the MAXIMA-1 experiment), then the number of maxima (or minima) in the observational map is

$$N_{max} \simeq 16 \left( \frac{f_{sky}}{0.003} \right) \left( \frac{\theta_{FWHM}}{1^\circ} \right)^{-2}. \quad (13)$$

According to [1,2] for MAXIMA-1 and BOOMERANG the antenna beam corresponds to  $FWHM \simeq 10'$ . This means that in the absence of the Doppler peaks in the power spectrum we can find 576 maxima on the corresponding maps. However one can find from Eq.(7)-(9) that the presence of Doppler peaks in the initial power spectrum changes the number of peaks in the map down to 271 for the mentioned above observational data. So, after our analysis we can conclude that the influence of the Doppler peaks leads to decrease of the number of hot and cold spots on the map by a factor  $\simeq 2$ . This result consists with the data of the MAXIMA-1 and BOOMERANG maps.

The next problem which we would like to discuss below is the following. How sensitive is the topology of  $\Delta T/T$  map to the amplitudes of the second  $A_2$  and third  $A_3$  Doppler peaks assuming that the amplitude and the position of the first one are known? To give answer to this question we compare  $\gamma(A_2, A_3)$  and  $N_{pk}(A_2, A_3)$  for the following models. In the first model we take the amplitude  $A_1$  corresponds to the data [1,2] and positions and widths of the next peaks in power spectrum are the following:  $l_1 = 210$  with the width  $d_1 = 95$ ,  $l_2 = 580$  with the width  $d_2 = 110$  and  $l_3 = 950$  with the width  $d_3 = 130$ . Corresponding plots are in Fig.1.

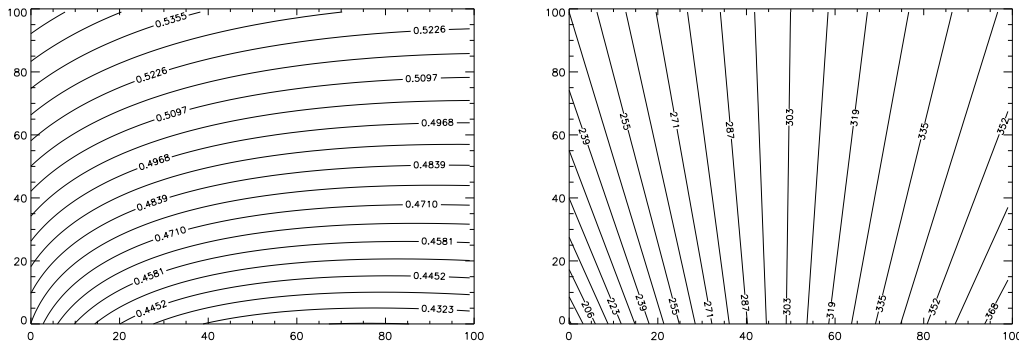


FIG. 1. The dependence of the  $\gamma(x, y)$  (left) and  $N_{pk}(x, y)$  (right) on the parameters  $x = 10^2 A_2/A_1$  (horizontal axes),  $y = 10^2 A_3/A_1$  (vertical axes). The numbers in the lines correspond to the values of  $\gamma(x, y)$  and  $N_{pk}(x, y)$ . Note that  $x = 26$  and  $y = 46$  corresponds to the MAXIMA-1 and BOOMERANG amplitude of the first, and two next Doppler peaks.

The second model (see plots in Fig.2) corresponds to a hypothetical situation when the amplitude of the first Doppler peak is two times smaller than in the previous case. As one can see from Eq(7)-(9) and Fig.1, Fig.2, in this second “toy” model the structure of the spectral parameters  $\gamma(A_2, A_3)$  and  $N_{pk}(A_2, A_3)$  changes drastically. The number of the maxima increases up to more than 420 while  $\gamma$  parameter conserves practically the same value:  $\gamma \simeq 0.4-0.47$ . This result is important for analysis of the global and local topology of the maps. In the BOOMERANG and MAXIMA-1 experiments the amplitude and position of the first Doppler peak in  $C_l$ -power spectrum are measured with 10% accuracy. That means that theoretical predictions of the number of the CMB peaks in the observational maps could change from 263 to 279 due to this 10% uncertainty. The difference in 16 peaks corresponds to  $\frac{\delta N}{N} \sim N^{-1/2}$  statistical fluctuations of the number of peaks  $N$  in the map practically without any essential changes of the  $\gamma$ -parameter. For other aspects of the distribution of the peaks in the maps see [7-9].

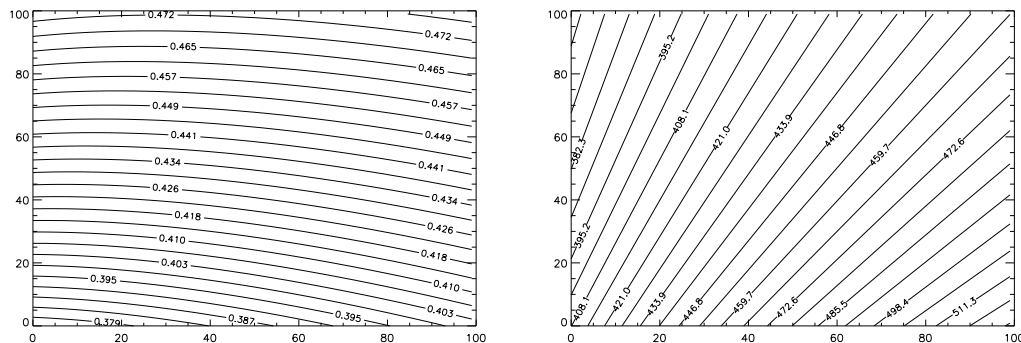


FIG. 2. The same as in Fig.1 but for a toy model with the amplitude of the first Doppler peak is two times less than in Fig.1

### III. STRUCTURE OF THE HIGH PEAKS OF THE CMB ANISOTROPY.

In this section we consider how the structure and shape of the high peaks in the observational maps change when one goes to higher angular resolution maps. In this case one can measure the structure of the  $\Delta T$ -field around a high peak with more details.

Can the future measurements reveal internal structure of the peaks which are found by BOOMERANG and MAXIMA-1? For example can the future measurements reveal new peaks in the fine structure inside the region around the  $\nu \simeq 2$  - peak down to the  $\nu = 0$ ? And if yes, what would be a typical height of such peaks? The answers to these questions depend on the peak-peak correlation in a high-resolution map. Two important properties of a random Gaussian field play a leading role in this problem. First, in the vicinity of a high maximum of a Gaussian field the random character of  $\Delta T(x, y)$  distribution is broken, and the shape of the peak is regular. The typical scale of such a regularity is, of course,  $\theta_*$  (see Eq.(2)). Second, as we mentioned above, the fractional variance in the peak number from one realization to another over a grid of area  $\Omega_p$  is related to the peak-peak correlation function  $C_{pk-pk}$  [6,9]:

$$\langle (\Delta N_{pk}^+)^2 \rangle / \langle N_{pk}^+ \rangle^2 = \langle N_{pk}^+ \rangle^{-1} + \int \frac{d\Omega_{\bar{q}} d\Omega_{\bar{q}'}}{\Omega_p^2} C_{pk-pk}(\bar{q} - \bar{q}'), \quad (14)$$

where  $\langle N_{pk}^+ \rangle = n_{pk}^+(\nu_t) \Omega_p$ ;  $n_{pk}^+(\nu_t)$  is the integrated number density of the maxima with height  $\nu$  above some threshold  $\nu_t$ . Note that the first term in Eq.(14) corresponds to the Poissonian distribution of peaks. Recently Heavens and Sheth [9] performed analytical and numerical calculations of the peak-peak correlation function and showed that  $C_{pk-pk}$  goes to zero at  $\theta < \theta_*$ , and reaches negative value  $C_{pk-pk} = -1$ , at  $\theta = 0$ . This result reflects the fact that the different high peaks cannot be located close to each other and, for example, two high peaks with the amplitudes  $\nu_1 \sim \nu_2 \sim 2 \div 2.5\sigma$  should be separated by the distance  $\theta \gg \theta_*$ . According to [9] the typical angular scale  $\theta_*$  for the most preferable  $\Lambda$ CDM cosmological models is close to 20 arcmin. This scale is twice greater than FWHM in the BOOMERANG and MAXIMA-1 experiments and 4 times greater than in the PLANCK-mission. However, it is worth noting, that inside the mentioned above region around the high peak there can exist up to  $\sim 10$  low amplitude peaks ( $\nu \leq 1$ ) in a high resolution map. These peaks are extremely important for the proof of the Gaussian statistics of a signal in such a map. Thus we can conclude that the isolated  $2 \div 2.5\sigma$  peaks which were found in the low-resolution BOOMERANG and MAXIMA-1 maps will reveal themselves as isolated peaks in the PLANCK map.

Let us come back to the discussion of the high peak at the location  $\delta = 58.6$  degrees; RA= 15.35 hours of the MAXIMA-1 map. The position of this peak practically does not depend on the higher angular resolution of the future PLANCK mission and its amplitude can be described as follows. Let us imagine that an ideal experiment with a  $\delta$ -function antenna beam finds the highest peak in the  $\Delta T$  map at the position  $(\bar{\delta}; \bar{RA})$ . An amplitude of such a peak measured in units of variance is:

$$\nu_{in} = \Delta T / \sigma_{0(in)}, \quad (15)$$

where  $\sigma_{0(in)}$  corresponds to Eq.(8) at  $\theta_A = 0$  and  $\xi = s$ . We suppose for simplicity that the distribution of  $\Delta T(x, y)$  around the point of maximum is Gaussian (more comprehensive consideration can be found in [6]) with the characteristic scales  $a$  and  $b = \kappa a$ ,  $\kappa$  is a constant:

$$\Delta T(x, y) = \nu_{in} \sigma_{0(in)} \exp\left(-\frac{x^2}{2a^2} - \frac{y^2}{2b^2}\right), \quad (16)$$

where the parameter  $a$  is proportional to the typical correlation scale of the initial signal. Following [6] we can describe a local shape of the peak of height  $\nu$ , measuring radial curvature  $\Gamma$  and “ellipticity”  $e$  using polar coordinates  $\bar{\theta}$  and  $\bar{\varphi}$ :

$$\delta(\bar{\theta}, \bar{\varphi}) = \sigma_{0(in)} \left[ \nu_{in} - \frac{1}{2} \gamma \Gamma \left( \frac{\bar{\theta}}{\theta_C} \right)^2 (1 + 2e \cos 2\bar{\varphi}) \right]. \quad (17)$$

Let us denote  $\bar{\theta}^2 = x^2 + y^2$  and  $\cos 2\bar{\varphi} = \frac{x^2 - y^2}{x^2 + y^2}$ . After that we find:

$$a^2 = \frac{\nu_{in} \theta_c^2}{(1 + 2e) \gamma \Gamma}; \quad b^2 = \frac{\nu_{in} \theta_c^2}{(1 - 2e) \gamma \Gamma}; \quad \kappa^2 = \frac{1 + 2e}{1 - 2e}. \quad (18)$$

In terms of eccentricity  $\epsilon = 2[e/(1 + 2e)]^{1/2}$  the last relation in Eq.(18) can be transformed to

$$\kappa^2 = 1/(1 - \epsilon^2). \quad (19)$$

Let us consider two experiments which measure the same part of the sky around a peak with different angular resolutions  $\theta_1$  and  $\theta_2$ . Suppose that  $\theta_1$  corresponds to the MAXIMA-1 FWHM and  $\theta_2$  corresponds to the PLANCK ( $\theta_1 \simeq 2\theta_2$ ). We denote an amplitude of the maximum in the low-resolution experiment by  $\nu_{maxima}$  and for the high-resolution experiment by  $\nu_{planck}$ . For such models an amplitude of the peak is

$$\widetilde{\Delta T}_j(x, y) = \frac{1}{2\pi\theta_j^2} \int dx' dy' \Delta T(x', y') \exp \left[ -\frac{(\bar{r} - \bar{r}')^2}{2\theta_j^2} \right], \quad (20)$$

where index  $j = 1, 2$  corresponds to  $\theta_1$  and  $\theta_2$ ,  $\bar{r}(x, y)$  and  $\bar{r}'(x', y')$  are vectors in the Cartesian coordinate system centered at the point of the maximum. The shape of  $\widetilde{\Delta T}_j(x, y)$  from Eq.(16) for the low- and high-resolution experiments is

$$\widetilde{\Delta T}_j(x, y) = \frac{\nu_{in} \sigma_{0(in)} ab}{[(a^2 + \theta_j^2)(b^2 + \theta_j^2)]^{1/2}} \exp \left[ -\frac{x^2}{2(a^2 + \theta_j^2)} - \frac{y^2}{2(b^2 + \theta_j^2)} \right]. \quad (21)$$

This curve determines parameter  $\xi_1^2 = (b^2 + \theta_1^2)/(a^2 + \theta_1^2)$  which we can measure in the vicinity of the peak at some threshold  $\nu_t \sigma_0^{(1)}$ , where  $\sigma_0^{(1)}$  is the variance of fluctuations in the low-resolution experiment. As a result the amplitude of the peak from Eq.(15) is

$$\nu_{maxima} \sigma_0^{(1)} = \frac{\nu_{in} \sigma_0^{(in)} \kappa}{\xi_1 (1 + \theta_1^2/a^2)}. \quad (22)$$

For the high-resolution experiment we obtain from Eq.(15)

$$\nu_{planck} \sigma_0^{(2)} \simeq \frac{\nu_{in} \sigma_0^{(in)} \kappa}{[(1 + \theta_2^2/a^2)(\kappa^2 + \theta_2^2/a^2)]^{1/2}}, \quad (23)$$

and while the difference between  $\sigma^{(in)}$ ,  $\sigma_0^{(1)}$  and  $\sigma_0^{(2)}$  is logarithmic only (see Eq.(8)) we have

$$\nu_{planck} \approx \nu_{maxima} \frac{\xi_1 (1 + 4\mu^2)}{[(1 + \mu^2)(\kappa^2 + \mu^2)]^{1/2}}, \quad (24)$$

where  $\mu = \frac{\theta_2}{a} < 1$ .

For example, for the MAXIMA-1 peak at the coordinates  $\delta = 58.6$  degrees,  $RA \simeq 15.35$  this ratio is  $\sim 1.2 \div 1.4$ . Taking into account this result  $\nu_1 \simeq 2 \div 3$  peaks in the MAXIMA-1 map will be transformed to higher peaks in the PLANCK map ( $\nu_2 \simeq 3 \div 4$ ),  $\theta_1 \simeq 2\theta_2$ . This conclusions are important for our discussions in the next section.

#### IV. STRUCTURE OF THE POLARIZATION FIELD AROUND THE POINTS WHERE POLARIZATION OF THE CMB SIGNAL VANISHES.

The structure of the polarization field and its auto- and cross-correlation with the anisotropy distribution on the sky has been studied in many papers (see for review [10]). Below we consider the structure of the polarization field around such singular points where  $P = 0$  in the CMB signal taking into account possible foregrounds and noise. This analysis can help in the estimation of a possible level of the foregrounds and noise in the future MAP and PLANCK polarization maps.

Of course, measurements of the CMB polarization around the points where it vanishes are a very difficult observational problem. However it is not necessary to go exactly to the point where  $Q^2 + U^2 = 0$  (where  $Q$  and  $U$  are Stokes parameters), because the structure of the polarization field can be determined by the pattern created by the flux lines around peculiar points. We note also that in spite of the fact that these points are distributed almost randomly over a map it is more probably to find them in the vicinities of high peaks of the  $\Delta T/T$  anisotropy. Indeed, in coming paper we will show that there is non-zero correlation between high maxima of anisotropy and singular points of polarization field. In this paper we consider the problem in the continues (non discrete) measurements of the  $Q$  and  $U$  values to reveal the main qualitative behaviors of the polarization field. The correspondingly consideration for pixelized maps see in [11]. We shall assume that in the observational map  $Q$  and  $U$  components of Stokes vector are the sum of the initial CMB signal  $(\bar{Q}, \bar{U})$  and the Gaussian noise  $(n_Q, n_U)$  which model the influence of pixel noise and polarized point sources on the primordial CMB signal. We shall assume also that statistical properties of the noises  $n_Q$  and  $n_U$  are identical and their correlation functions are  $C_{ij}^Q = C_{ij}^U = \sigma_n^2 \delta_{ij}$ , where  $\sigma_n^2$  is the variance. This means that we neglected the correlation between noise of different pixels. Under the assumption mentioned above we can expand  $\bar{Q}$  and  $\bar{U}$  near the points where  $\bar{Q} = \bar{U} = 0$  as follows:

$$\begin{aligned}\bar{Q} &\approx q_1 x + q_2 y \\ \bar{U} &\approx u_1 x + u_2 y,\end{aligned}\tag{25}$$

where  $x$  and  $y$  are Cartesian coordinates of the system centered at the zero-point of polarization;  $q_1, q_2$  and  $u_1, u_2$  are the corresponding partial derivatives. Thus the modulus of the polarization vector  $P^2 = Q^2 + U^2$  is

$$P^2 = \bar{P}^2 + 2(\bar{Q}n_Q + \bar{U}n_U) + n_Q^2 + n_U^2,\tag{26}$$

where  $\bar{Q}$  and  $\bar{U}$  correspond to Eq.(25).

Lets us firstly describe the model when  $n_Q$  and  $n_U$  are negligible with respect to the regular functions  $\bar{Q}$  and  $\bar{U}$ . This situation takes place when  $\bar{Q}^2 + \bar{U}^2 \gg n_Q^2 + n_U^2$  or  $\bar{P}^2 \gg \sigma_n^2$ , where  $\sigma_n^2$  is variance of the noise and in Eq.(26) we can neglect all terms excluding  $\bar{P}^2$ . In such a case we obtain from Eq.(26):

$$P^2 = \bar{P}^2 = \sum_{i,j=1}^2 a_{ij} x^i y^j,\tag{27}$$

where  $a_{11} = q_1^2 u_1^2$ ;  $a_{22} = q_2^2 u_2^2$ ;  $a_{12} = a_{21} = q_1 q_2 + u_1 u_2$ . Rotating the coordinate system through the angle  $\text{tg}2\psi = \frac{2a_{12}}{a_{11} - a_{22}}$  one can transform Eq.(27) to the ‘‘standard’’ form:

$$\bar{P}^2 = Ax^2 + By^2,\tag{28}$$

where  $A = \frac{1}{2} [a_{11} + a_{22} + \sqrt{1+t^2}(a_{11} - a_{22})]$ ;  $B = \frac{1}{2} [a_{11} + a_{22} - \sqrt{1+t^2}(a_{11} - a_{22})]$ ;  $A \cdot B > 0$ ;  $t = \text{tg}2\psi$  and  $x$  and  $y$  are the coordinates after rotation.

As one can see from Eq.(28) the condition  $\bar{P} = \text{const}$  determines the ellipses with a peculiar isolated point inside them  $\bar{P}^2 = 0$ . Therefore the structure of the field  $P^2(x, y)$  around points  $\bar{P}^2 = 0$  for the case  $\bar{P}^2 \gg n_Q^2 + n_U^2$  is rather simple. But when we come close enough to the point  $\bar{P}^2 = 0$  this condition will be violated because the level of noise is approximately constant  $> 0$  near the point  $\bar{P}^2 = 0$ . Now in Eq.(26) we take into account the second term but neglect  $n_Q^2 + n_U^2$ , so

$$P^2 - \bar{P}^2 = 2(\bar{Q}n_Q + \bar{U}n_U).\tag{29}$$

As one can see from Eq.(29) the function  $f = P^2 - \bar{P}^2$  is a nonuniform random function due to a regular character of  $\bar{Q}$  and  $\bar{U}$  components in the vicinity of the peculiar point and the randomly distributed noise. From Eq.(29) we can estimate the variance of the random function  $f$ :

$$\sigma_f^2 \approx 4\bar{P}^2 \sigma_n^2, \quad (30)$$

which depends on the module  $\bar{P}(x, y)$ . From Eq.(30) we can define more precisely the limits of applicability of the approximation Eq.(29):  $\sigma_f^2 > \sigma_n^4$  and therefore

$$\sigma_n < \frac{1}{2}\bar{P}. \quad (31)$$

This relation shows that influence of the noise on the contour lines around peculiar point of polarization field becomes stronger when we come closer to the point  $\bar{P} = 0$ .

Finally at the very vicinity of the point  $\bar{P}^2 = 0$  we come to the region where  $\sigma_n^2 > \frac{1}{4}\bar{P}^2$  and for this region we have the approximation

$$P^2 = n_Q^2 + n_U^2. \quad (32)$$

If  $n_Q$  and  $n_U$  are independent random Gaussian functions then  $P = \sqrt{n_Q^2 + n_U^2}$  is the Rayleigh random process with pdf  $\Phi(U)$ :

$$\Phi(U) = \frac{U}{\sigma_n^2} \exp\left(-\frac{U^2}{2\sigma_n^2}\right). \quad (33)$$

As we can see from Eq.(33) the probability to find the point with zero level of polarization inside the area  $\sigma_n^2 > \frac{1}{4}\bar{P}^2(x, y)$  is proportional to  $\bar{P}^2/(4\sigma_n^2)$  and goes to zero if  $\bar{P} \rightarrow 0$ . This means that pixel noise or (and) polarized point sources destroy the structure of the field around nonpolarized points of the primordial signal and in principle remove this peculiarities from the map. Thus the regions around the peculiar points of polarization are very sensitive to the pixel and point sources noises. The structure of the polarization field around such points gives us the information about the variance and statistical properties of the noises and can be used for filtration of such noises. We discuss this problem in details in [11] for filtration of the polarization maps.

## V. CONCLUSIONS

New theoretical methods have been developed recently to provide the analysis and exploiting the new and forthcoming CMB data sets. The BOOMERANG and MAXIMA-1 missions have discovered a lot of “hot” spots of the CMB radiation on the sky. These peaks in  $\Delta T$ -distribution on the sky play a role of “standard” sources of the CMB anisotropy signal for future balloon and satellite experiments with more sensitive radiometers and higher angular resolutions. The new theoretical methods are developing now to provide the analysis and predictions the new and forthcoming CMB data sets.

## VI. ACKNOWLEDGMENTS

D.Novikov is grateful to the staff of TAC for providing excellent working conditions during his visit. The authors are grateful to Per Rex Christensen and Andrei Doroshkevich for useful discussions. This investigation was supported in part by the Danish Natural Science Research Council through grant No. 9701841 and also in part by the grants INTAS- 1192 and RFFI- 17625. Authors are grateful to Danmarks Grundforskningsfond through its support for establishment of the Theoretical Astrophysics Center. D.Novikov acknowledges Board of the Glasstone Benefaction.

- [1] De Beranrdis, P. et al., Nature **404**, 955 (2000).
- [2] Hanany, S. et al., astro-ph/0005123, (2000).
- [3] Tegmark, M. and G. Efstathiou, MNRAS **281**, 1297, (1996) .
- [4] Lahave, O.,S.L. Bridle, M.P. Hobson, A.N. Lasenby and L. Sodr'e Jr., astro-ph/9912105, (1999).



- [5] Bunn, E.F., Y. Hoffman and J. Silk, astro-ph/9509045, (1995).
- [6] Bond J.R. and G. Efstathiou, MNRAS, **226**, 655, (1987).
- [7] Zabolin, N. and P.Naselsky, Soviet Astron. **29**, 614, (1985)
- [8] Naselsky, P., I.Novikov, Yu. Parijskij and P.Tcibulev, Int.J. of Modern Physics **8**, n5, 581, (1999).
- [9] Heavens, A.F. and R.K.Sheth, astro-ph/9904307, (1999), MNRAS in press.
- [10] Rees. M., ApJ, **153** L1, (1968).;
  - Basco, M. and A.Polnarev, Soviet Astron. **24**, 3, (1979);
  - Polnarev, A., Soviet Astron. **62**, 1041, (1985);
  - Naselsky, P. and A.Polnarev, Astrophysics **26**, 543, (1987);
  - Coulson, P., R.Grittenden and N.Turok, Phys. Rev. Lett. **73**, 2390, (1994);
  - Ng, K.L.and K.W.Ng,Phys. Rev. D. **51**, 364, (1995);
  - Zaldarriaga, M. and D.Harari, Phys. Rev. D. **52**, 3276, (1995);
  - Jungman, G., M.Kamionkowski, A.Kosowsky and D.Spergel, Phys. Rev. D. **54**, 1332, (1996);
  - Novikov, D. and H. Jorgensen, ApJ, **471** , 521, (1996);
  - Zaldarriaga, M. and U.Seljak, Phys. Rev. D, **55**, 1830, (1997);
  - Arbuzov,P., E.Kotok, P.Naselsky and I.Novikov, Int. J. of Modern Physics D, **6**, 515, (1997);
  - Naselsky, P. and D.Novikov, ApJ, **507**, 31, (1998);
  - Dolgov, A., A.Doroshkevich, D.Novikov and I.Novikov, Int. J. of Modern Physics D, **8**, 189, (1999),
  - Hu,W. and M.White, astro-ph/970647 (2000).
- [11] Naselsky, P., D. Novikov and I.Novikov, IAUS 201E.12N.(2000);
  - Naselsky, P., D. Novikov, I. Novikov, J. Silk, Proceedings of the IAUs 201, in press, (2000).